Vietnam Journal of Science and Technology ***62*** *(6) (2024) 1119-1133*
doi:10.15625/2525-2518/58/6/19166

Intuitive data and image analysis about the microstructure of the liquid alumina system

Mai Thi Lan*, Nguyen Thi Thanh Ha, Nguyen Thu Nhan, Nguyen Van Hong

Faculty of Engineering Physics, Hanoi University of Science and Technology, No. 1, Dai Co Viet Str., Hai Ba Trung Dist., Ha Noi, Viet Nam

*Email: *lan.maithi@hust.edu.vn*

Received: 12 October 2023; Accepted for publication: 29 October 2024

Abstract. The models of the Al_2O_3 system in a liquid state over broad ranges of pressure from 0 to 100 GPa are built by Molecular Dynamics simulation (MDs). This research gives useful knowledge about the microstructural properties of liquid alumina systems through insight 3D visualization. Intuitive data and image analysis methods are applied to clarify the network structure, the local environment of Al and O atoms, and the linkage among the polyhedra in the network structure of the Al_2O_3 system at different pressures. The structural compaction mechanism of Al_2O_3 oxides under high pressure is also discussed in this paper.

Keywords: Alumina Al_2O_3, the local environment, MD simulation, visualization.

Classification numbers: 2.9.2, 2.9.4.

1. INTRODUCTION

Alumina (Al_2O_3) has received great attention from materials researchers due to its good properties such as high melting and boiling point, excellent thermal resistive properties, high hardness, and good mechanical and compressive strengths. Therefore, alumina is widely applied in many fields such as ceramics and glass, refractories, biomedical applications, electronics, and construction materials. In catalysis, due to its high mechanical strength, transition alumina is used as catalysts and most widely as catalytic supports with low production cost [1, 2]. The structure of Al_2O_3 in the liquid state is also of interest because Al_2O_3 is an important component of aluminosilicate materials, which are the main components of the Earth's mantle [3]. Knowledge of the structural properties of the Al_2O_3 system at the atomic level under high temperature and pressure conditions is necessary for understanding the geologically relevant change of Earth's mantle, the nature of Earth's interior, as well as the fabrication of new materials with desirable properties. Hence, the Al_2O_3 system has been studied by experiment, theory, and simulation for a long time. When studying Al_2O_3 at high pressure by using density functional theory [4], *ab initio* simulations, and high-pressure experiments in a diamond anvil cell [5], the results showed that there is a new stable phase of Al_2O_3 with post-perovskite structure. Its stability will increase with high pressures. Al_2O_3 has the $CaIrO_3$-type structure at pressures above 130 GPa. The electronic structure of gamma alumina is similar to the one of alpha alumina and amorphous Al_2O_3 [6]. Experimental [7] reports the Al-O and O-O nearest

distances of 1.76 Å and 3.08 Å, respectively. The Al coordination changes from octahedral to tetrahedral in liquid and supercooled Al_2O_3 on melting. The mean Al-O coordination number is about 4.4. Using X-ray and neutron diffractions [8], Lampartera and R. Kniep indicate that the structure of amorphous Al_2O_3 is constructed by AlO_4 tetrahedra, and these AlO_4 link each other via the corner sharing oxygen atoms. The Al-O bond length is about 1.8 Å. The O-O distance is from 2.91 to 2.94 Å. The Al-O-Al bond angle between two the tetrahedra is about 125^0. The neutron scattering results [9] show that the liquid alumina is mainly built up by AlO_4 (62 %) and AlO_5 (24 %). The octahedral aluminum site AlO_6 is only about 2 %. The Al-O distance is about 1.78 Å. Skinner *et al.* have presented the results of the structure of liquid alumina near its melting point (2400 K) [3]. The structure of liquid alumina consists of AlO_x polyhedra at ambient conditions, in which AlO_4 and AlO_5 units are predominant. AlO_3 and AlO_6 units account for only minor fractions. The Al-O distance is about 1.77-1.78 Å. There are about 83% fraction of Al-O-Al linkages related to the corner-sharing bond which is similar to the results of the work [3]. On the other hand, in the study [10], the authors showed that the AlO_4 tetrahedra are dominant in the structure of amorphous Al_2O_3, but there is still a co-existence of AlO_5 and AlO_6 units in the structure. The fraction of AlO_5 and AlO_6 units in amorphous Al_2O_3 is more than in the liquid. The NMR studies [11] showed that the structure of amorphous Al_2O_3 is built by AlO_4, AlO_5, and AlO_6 units with by fractions of 55 %, 42 %, and 3 %, respectively. Al_2O_3 oxide is one of the simplest covalent oxides. The pressure significantly affected the mechanical, densification properties, and microstructures of the Al_2O_3 ceramics [12]. However, due to its high melting point temperature (the melting of Al_2O_3 at 0 GPa is about 2327 K [7], 2389 K [13], and 2200 K [14]), experimental studies are difficult when studying Al_2O_3 in the liquid state, especially at high pressure. Thus, many details about its atomic structure and physical properties at high temperatures and pressure remain unknown. Hence, simulation is still an effective tool to support experimental methods and elucidate the above problems. The simulation studies [15-18] illustrated that at low pressure, the structure of Al_2O_3 contains predominant AlO_4 and AlO_5 units. At high pressure, the structure of Al_2O_3 consists of mainly AlO_5 and AlO_6 units. There is a transition from the tetrahedral structure at low pressure to the octahedral structure at high pressure. This result is in good agreement with the first principle calculation [19] as well as experimental studies [3, 8]. At the density of 3.175 g/cm^3 and temperature of 2200 K, the Al-O, Al-Al, and O-O bond lengths in liquid Al_2O_3 are about 1.75 Å, 3.15 Å, and 2.75 Å, respectively. The O-Al-O and Al-O-Al bond angle distribution has a peak at 95° and 115°. The O-Al-O bond angle in AlO_4 units is about 109.47° [16]. Using MD simulation, the authors clarified the structural heterogeneity in liquid Al_2O_3 [20, 21] and indicated the existence of free-volume regions in liquid Al_2O_3 under compression up to 100 GPa through the Voronoi analysis [21].

In this contribution, the MDs of liquid Al_2O_3 system in the wide range pressure from 0 to 100 GPa are reported. Our main goal is to investigate in detail the microstructure, distribution of different structural regions in the model, and the densification mechanism of liquid Al_2O_3 under compression through intuitive data and image analysis methods.

2. COMPUTATIONAL PROCEDURE

We have performed MDs of liquid Al_2O_3 system in the wide range of pressure from 0 to 100 GPa. Simulation is conducted for 5500-atom models using Born-Meyer pair interaction potentials with periodic boundary conditions. The detail about this potential described in [17]. Initial configuration is generated by randomly placing all atoms in a cubic box with periodic boundary conditions. This sample is heated to 5000 K and equilibrated at this temperature to get

a properly equilibrated liquid and remove the effect of remembering the initial configuration. Then it cooled down to the desired temperature with a cooling rate of 2 K/ps. A well-equilibrated model (M0) has been constructed at the desired temperature and ambient pressure. The time consumed to obtain this model is about 10^6 MD steps. Then, we have calculated the total radial distribution function (RDF) of liquid Al_2O_3 models and compared the results of the total RDF function with the previous work to assure reliability of constructed model. Namely, the results of the total RDF of liquid Al_2O_3 are compared with experimental data of Ansell [7] and Skinner's Neutron experiment [8] are shown in Figure 1.

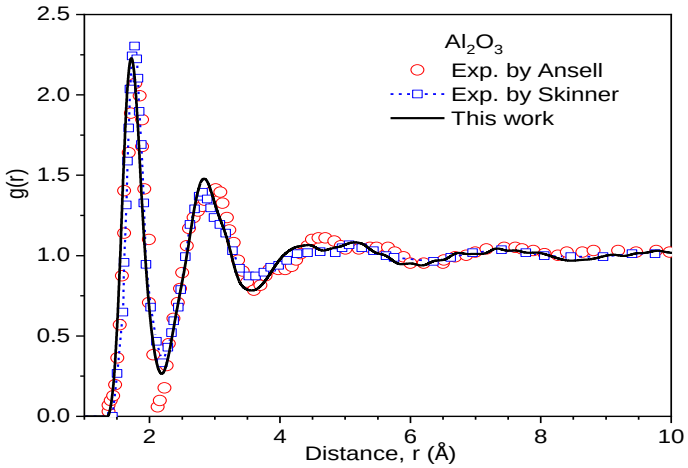

Figure 1. The total radial distribution function of liquid Al_2O_3.

The results showed that there is a good agreement of the shape, amplitude and position of the peaks, thus the constructed model is reliable. Next, to investigate liquid Al_2O_3 system under compression, we prepared 11 other models (M1-M11) by compressing the M0 model to desired densities and consequent long relaxing in *N-P-T* ensemble until the equilibrium is reached by checking the total energy and structural characteristics. The microstructural characteristics of interest are collected via data mining from MD data and 3D visualization techniques.

3. RESULTS AND DISCUSSION

The Al-O, Al-Al, and O-O pair radial distribution function (PRDF) of the constructed model Al_2O_3 is shown in Figure 2. At ambient pressure, the Al-O PRDF has a peak at a location of 1.68 Å. The peak tends to shift slightly to the right and the height decreases as pressure increases. At 100 GPa, the peak is located at a position of 1.70 Å. This reveals that the average Al-O bond lengths increase slightly under compression. The Al-Al and O-O PRDF shows that at ambient pressure, it has a peak at around 3.22 Å and 2.86 Å, respectively. Under compression, the PRDF shifts strongly to the left. At 100 GPa, the peak locates at around 2.88 Å and 2.52 Å, respectively. It means that the Al-Al and O-O bond length decrease with increasing pressure. Thus, the first peak position of Al-O, Al-Al, and O-O pairs indicate their average bond distance. The pressure dependence of the first peak position of these pairs is demonstrated in Figure 3a. It can be seen that, the O-O and Al-Al distance decreases significantly as pressure increases. Meanwhile, the Al-O distances increase slightly in the 0-100 GPa range. This reveals that the densification mechanism in liquid Al_2O_3 is mainly due to the decrease of O-O and Al-Al

distance. We analyzed the first peak height of the PRDF as a function of pressure shown in Figure 3b.

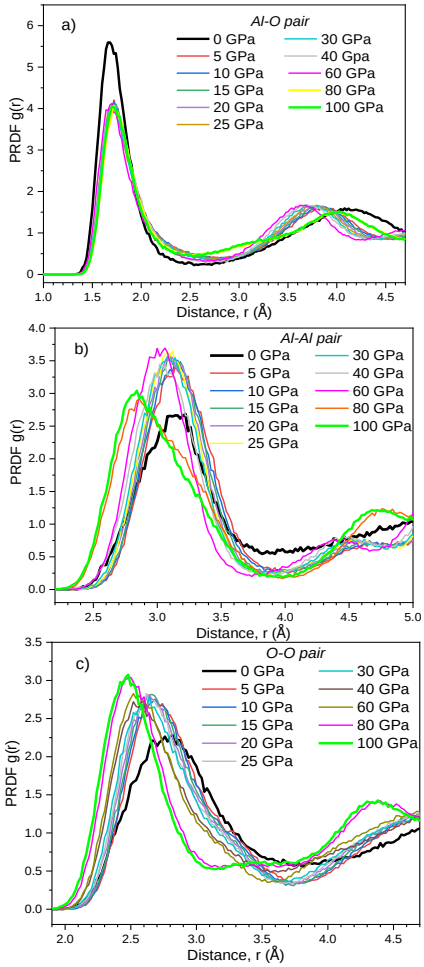

Figure 2. The PRDF of liquid Al_2O_3 model at different pressure.

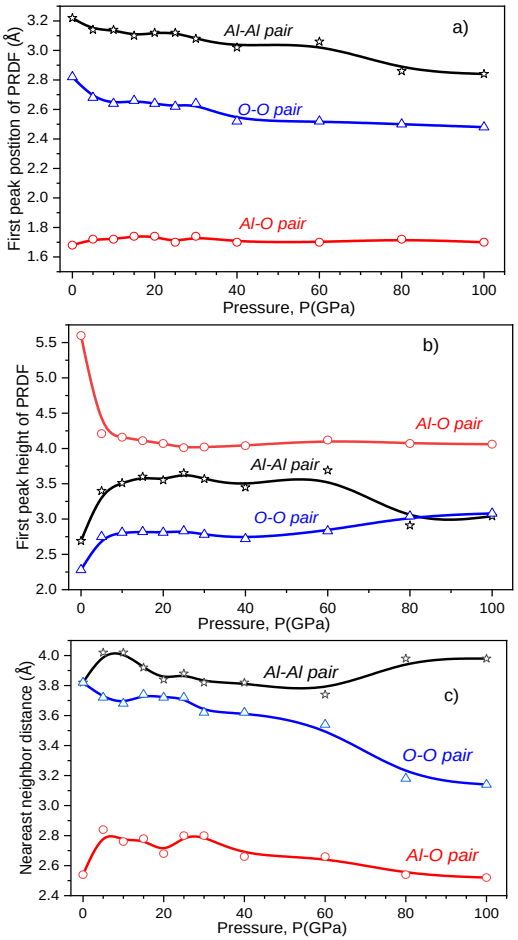

Figure 3. The first peak position (a), the peak height (b) and nearest neighbor distance (c) of PRDF.

It shows that the first peak height of Al-O PRDF decreases strongly in the 0-5 GPa range and then decreases slightly with pressure. It means that the local environment surrounding Al atoms changed, and the short-range order structure decreased with pressure, especially in the 0-5 GPa range. Meanwhile, the first peak height of Al-Al and O-O PRDF tends to increase in the considered pressure range. This means that the intermediate-range order structure changed significantly under compression. We calculated the pressure dependence of the nearest neighbor distance of Al-O, Al-Al, and O-O pairs that are shown in Figure 3c. It reveals that the nearest neighbor distance of Al-O pairs is around 2.50-2.60 Å in the considered pressure range. The nearest neighbor distance of O-O pairs is about 3.80 Å at ambient pressure and it decreases to 3.20 Å at 100 GPa. The nearest neighbor distance of the Al-Al pair increases slightly from around 3.80 Å at ambient pressure to 4.00 Å at 100 GPa. Thus, the nearest neighbor distance of

Al-O pairs depends on pressure. This once again reveals that the structure of Al_2O_3 change strongly under compression and the change relate to the decrease in the O-O distance and the increase of Al-Al distance.

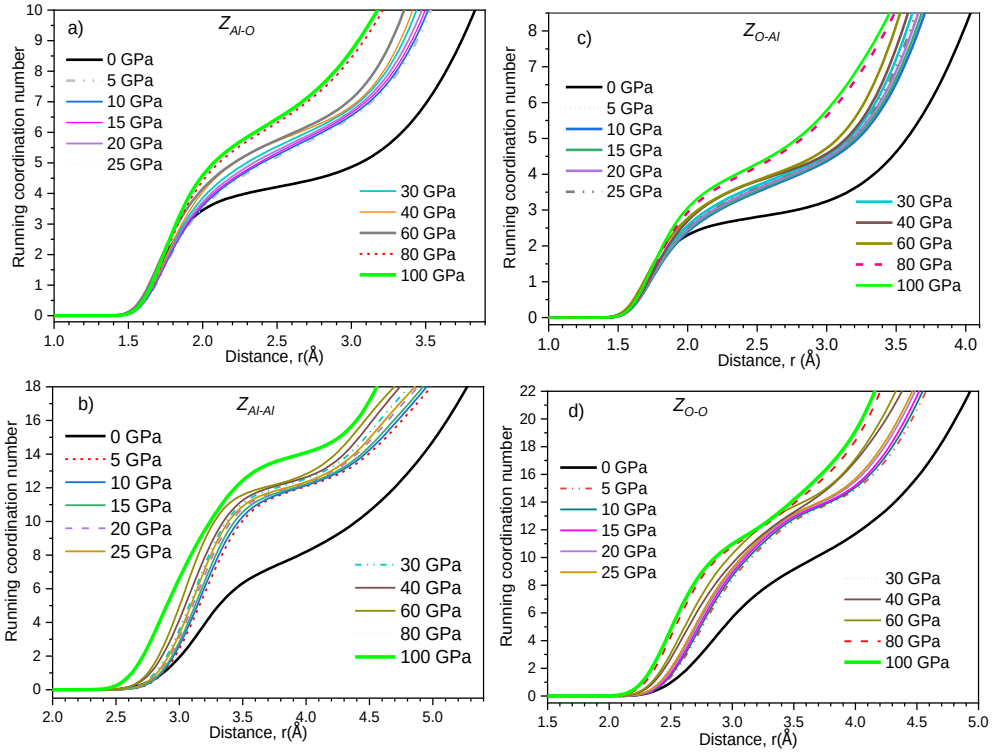

Figure 4. The RCN at different pressure.

Table 2. The mean CNs at different pressure

Pressure, P (GPa)	*Al-Al*	*Al-O*	*O-Al*	*O-O*
0	7.70	4.25	2.83	10.61
5	11.74	5.30	3.53	13.94
10	11.80	5.36	3.57	14.03
15	11.89	5.43	3.62	14.14
20	11.98	5.50	3.67	14.31
25	12.03	5.55	3.70	14.41
30	12.21	5.62	3.75	14.67
40	12.31	5.79	3.86	15.14
60	12.41	5.83	3.89	15.25
80	13.77	6.44	4.29	16.24
100	13.78	6.56	4.38	16.70

Figure 4 shows the running coordination number (RCN) of Al-O, Al-Al, and O-O pairs at different pressures. The average coordination number (CN) of Al-O (Z_{Al-O}), Al-Al (Z_{Al-Al}), and O-

O (Z_{O-O}) is determined from the first plateau of the curve in the RCN of Al-O, Al-Al, and O-O pairs, respectively. The average coordination numbers Z_{Si-O} and Z_{Al-O} are listed in Table 2. From Figure 4 and Table 3, it can be seen that at ambient pressure, each Al atom has an average of 7.7 Al atoms and 4.25 O atoms. And each O atom has an average of 2.83 Al atoms and 10.61 O atoms. Under compression, the local environment of all atoms changes strongly. The curve in the RCN has a significant change. The height of the shoulder tends to increase and change significantly within the scale of the first minimum distance. At 100 GPa, each Al atom has an average of 13.78 Al atoms and 6.56 O atoms. Each O atom has an average of 4.38 Al atoms and 16.70 O atoms. It means that the average CN increases with pressure. This reveals that the rearrangement via the increased coordination is the densification mechanism of Al_2O_3 liquid. The network structure can be seen by analyzing the CN distribution of all atomic pairs and 3D visualization of the spatial distribution of AlO_x polyhedral (x = 4 - 7) and O-Al_y linkages (y = 2 - 5). Figure 5a shows that, at ambient pressure, each Al atom is mainly surrounded by four oxygen atoms that form an AlO_4 tetrahedron. The fraction of AlO_4 tetrahedra is about 65.05 %. In the pressure region from 5 - 10 GPa, most of the loss of AlO_4 is accounted for by an increase in AlO_5 and AlO_6. With further increasing pressure, AlO_6 and AlO_7 replace AlO_4 and AlO_5. At 100 GPa, the fraction of AlO_6 and AlO_7 reach about 47.67 % and 38.38 %, respectively. It indicates the transformation from AlO_4 tetrahedra to AlO_6 octahedra and AlO_7 polyhedra network structure in Al_2O_3 liquid under compression.

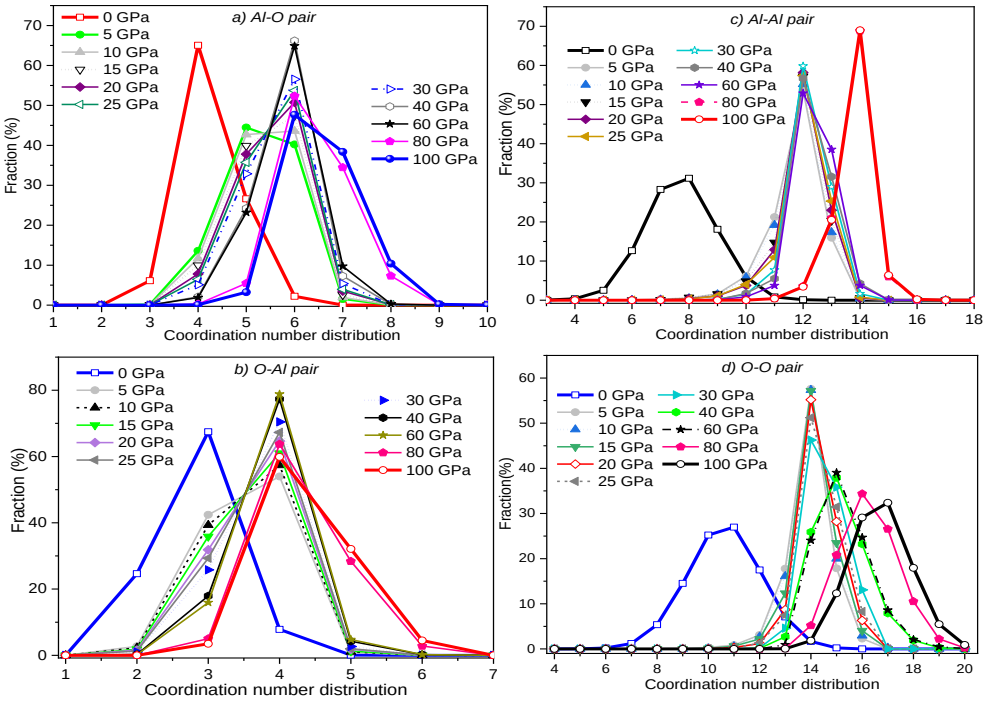

Figure 5. The CN distribution of all atomic pairs at different pressure.

For the O-Al pair (Figure 5b), at ambient pressure, there are 24.64 % of the O atoms are twofold coordinated by Al atoms (OAl_2) but around 67.45 % of OAl_3 tri-cluster that O atoms are surrounded by three Al atoms. The proportion of OAl_2 and tri-cluster decreases strongly and the CN of O atoms increases as pressure increases. At 100 GPa, each O atom is surrounded by 4 and

5 Al atoms forming OAl_4 and OAl_5. The percentage of OAl_4 and OAl_5 reaches about 59.88 and 32.12 %, respectively. Similarly, for Al-Al and O-O pairs (Figure 5c, d), the CN of them increases with pressure. Around the Al has mainly 7, 8, and 9 other Al atoms at ambient pressure and increase to 13, and 14 at 100 GPa. Around the O has mainly 9, 10, and 11 other O atoms at ambient pressure and increases to 16, and 17 at 100 GPa. Generally, there is an increase in the CN of all atomic pairs under compression. This again demonstrates that the increased coordination is the densification mechanism of the Al_2O_3 system under compression. From the above analysis, we can conclude that the liquid Al_2O_3 system comprises species AlO_x polyhedra (x = 4-7) with the fraction of polyhedra varied with pressure. At ambient pressure, the Al_2O_3 liquid is like a mixture of species AlO_4 tetrahedra and AlO_5 pentahedra, in which the fraction of the AlO_4 tetrahedra network is the largest. At high pressure up to 100 GPa, the Al_2O_3 liquid consists of species AlO_6 octahedra, AlO_7, and AlO_8 polyhedra, in which AlO_6 octahedra and AlO_7 polyhedra network are dominant.

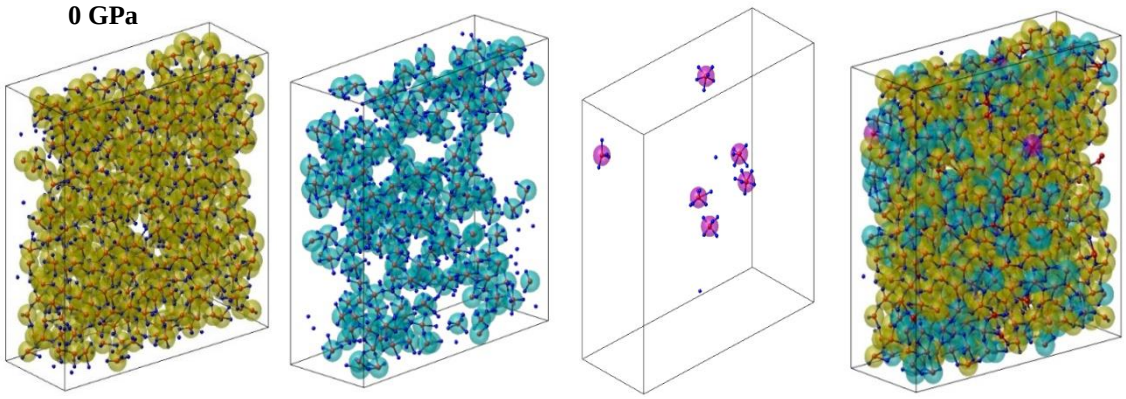

Figure 6. The 3D visualization of the distribution of coordination polyhedral (CP) in liquid Al_2O_3 model at 0 GPa (AlO_4 tetrahedra in yellow, AlO_5 pentahedra in cyan, AlO_6 octahedra in pink and all AlO_x (x = 4, 5, 6) polyhedra that correspond to the snapshots from left to right.

These results are further confirmed by the 3D visualization technique of the spatial distribution of AlO_x coordination polyhedral (CP) in Al_2O_3 liquid at different pressures as shown in Figure 6 - 10. Figure 6 indicates that at ambient pressure, the regions with AlO_4 tetrahedra in yellow are the most dominant (see Figure 6a). Next are the regions with AlO_5 pentahedra in cyan (see Figure 6b). Finally, the regions with AlO_6 octahedra in pink are negligible (see Figure 6c). Thus, the visual image shows that the structure of Al_2O_3 liquid consists of three regions with different short-range order structures (see Figure 8d). These regions are unevenly distributed in the model, hence the structure of Al_2O_3 liquid is heterogeneous. Similarly, the visual image of the structure of Al_2O_3 liquid at 10, 30, 60, and 100 GPa also illustrates the short-range order structure heterogeneity. At 10 GPa, the structure of Al_2O_3 comprises AlO_4 tetrahedra in yellow, AlO_5 pentahedra in cyan, and AlO_6 octahedra in pink (Figure 7). In which, the yellow regions are shrunk, and the cyan and pink regions are expanded and dominant. At 30 GPa, the regions with AlO_6 octahedra in pink are dominant while the regions with AlO_4 tetrahedra in yellow are negligible (Figure 8).

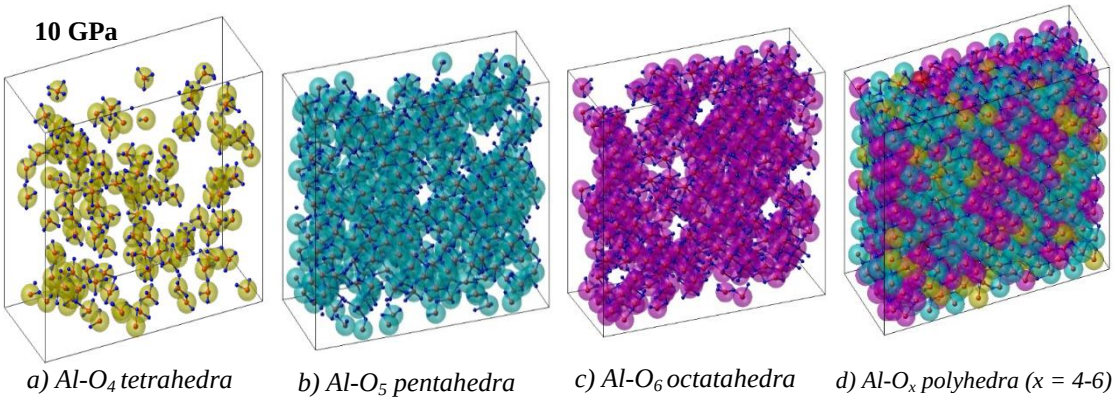

Figure 7. The 3D visualization of the distribution of CP in liquid Al_2O_3 model at 10 GPa (AlO_4 tetrahedra in yellow, AlO_5 pentahedra in cyan, AlO_6 *octahedra* in pink and all AlO_x (x = 4, 5, 6) polyhedra that correspond to the snapshots from left to right.

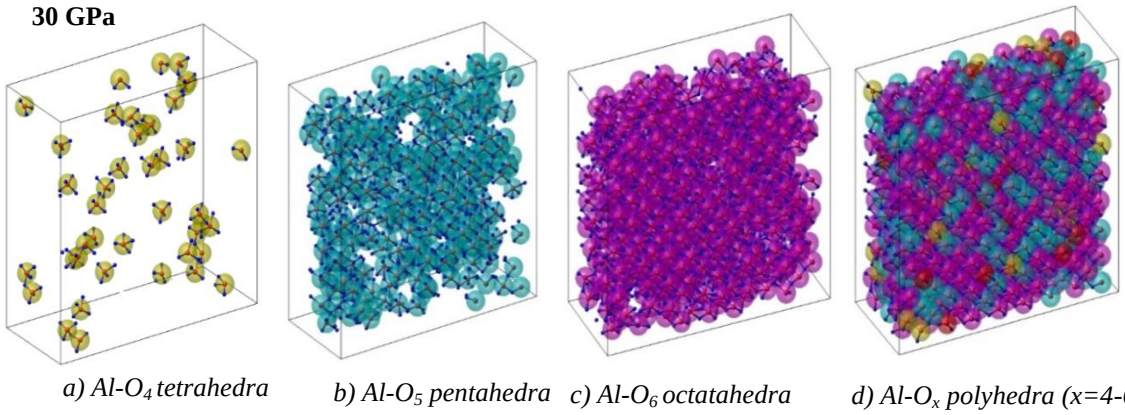

Figure 8. The 3D visualization of the distribution of CP in liquid Al_2O_3 model at 30 GPa (AlO_4 tetrahedra in yellow, AlO_5 pentahedra in cyan, AlO_6 octahedra in pink and all AlO_x (x = 4, 5, 6) polyhedra that correspond to the snapshots from left to right.

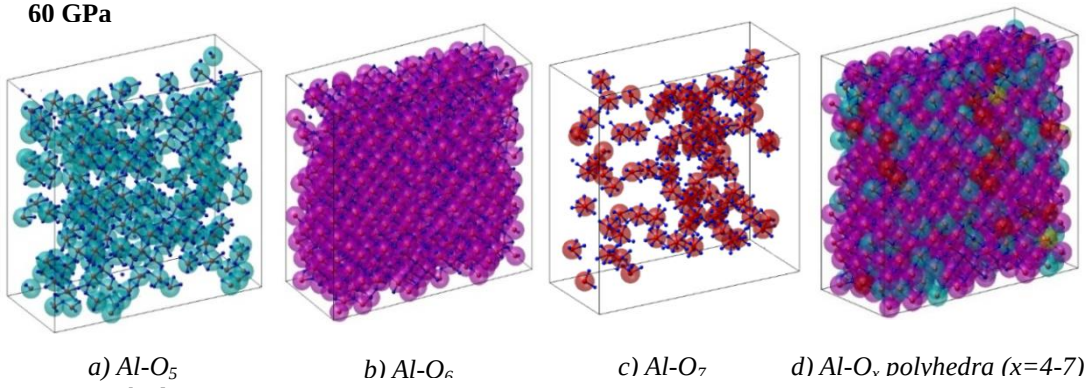

Figure 9. 3D visualization of the distribution of CP in liquid Al_2O_3 model at 60 GPa (AlO_4 tetrahedra in yellow, AlO_5 pentahedra in cyan, AlO_6 *octahedra* in pink and all AlO_x (x = 4, 5, 6) polyhedra that *correspond to* the snapshots from left to right.

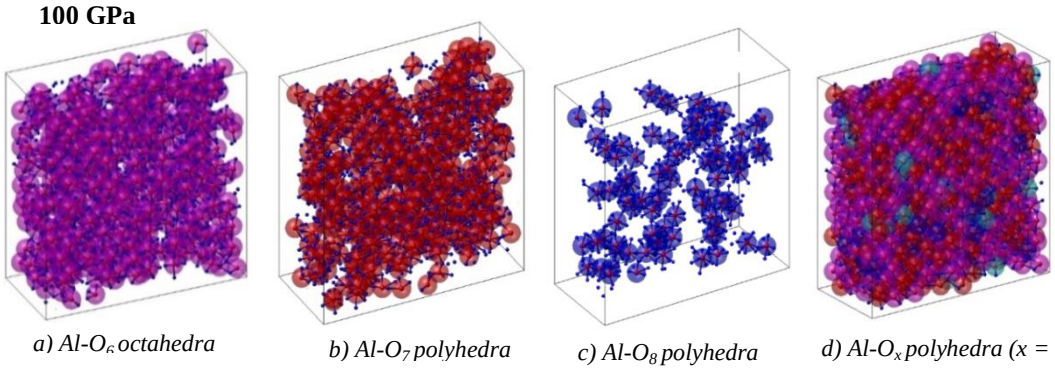

Figure 10. The 3D visualization of the distribution of CP in liquid Al_2O_3 model at 100 GPa (AlO_6 octatahedra in pink, AlO_7 polyhedra in red, AlO_8 polyhedra in blue, and all AlO_x polyhedra (x = 6, 7, 8) that correspond to the snapshots from left to right.

When pressure increases further, the yellow regions of AlO_4 tetrahedra disappear, the cyan regions of AlO_5 pentahedra continue are shrunk and begin appearing the regions with higher coordination polyhedra (Fig. 9). At 100 GPa, the structure of liquid Al_2O_3 consists of three main regions with AlO_6 octahedra in pink, AlO_7 polyhedra in red, and AlO_8 polyhedra in blue, in which the pink and red regions make up the majority (Fig.10). Therefore, the visual results show good agreement with the above structural analysis. The short-range order structure in Al_2O_3 liquid is heterogeneous. It is a mixture of the regions AlO_x polyhedra (x = 4 - 8) with the percentage varied with pressure. Useful information about the linkage between two adjacent AlO_x polyhedra that relate to intermediate-range order structure is provided by the distribution of O-Al linkages (Fig. 11). According to this figure, most of the linkages are O-Al_2 and O-Al_3 at ambient pressure. The O-Al_4 linkages account for a small fraction. As the pressure increases, the fraction of O-Al_2 and O-Al_3 linkages decreases, while the fraction of O-Al_4, O-Al_5, and O-Al_6 linkages increases. At 100 GPa, the percentage of O-Al_4 and O-Al_5 linkages becomes considerable. It means that the intermediate-range order structure changes with pressure. On the other hand, as mentioned above, the AlO_4 tetrahedra and AlO_5 pentahedra network are dominant at ambient pressure while the AlO_6 octahedra and AlO_7 polyhedra network are considerable at 100 GPa. Therefore, we can conclude that O-Al_2 and O-Al_3 linkages correspond to the AlO_4 and AlO_5 polyhedra networks. The O-Al_4 and O-Al_5 linkages correspond to the AlO_6 and AlO_7 polyhedra networks. Certainly, with increasing pressure, the change in the percentage of AlO_x polyhedra relates to a change of short-range order structure that should be accompanied by the change of intermediate-range order structure (the change of linkages among adjacent AlO_x polyhedra). The different intermediate-range order structure is clearly highlighted with different colors through the 3D visualization technique of the spatial distribution of O-Al_y linkages in Al_2O_3 liquid at different pressures (Figs. 12 -1 6).

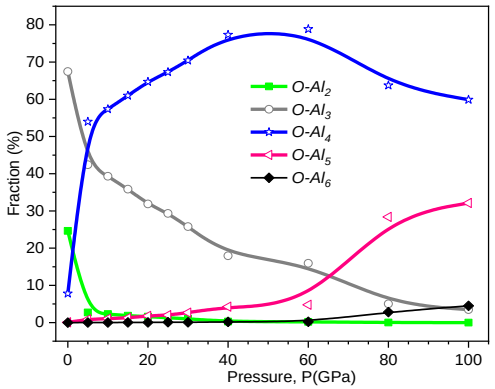

Figure 11. The distribution of O-Al_y (y = 2-6) linkages.

0 GPa

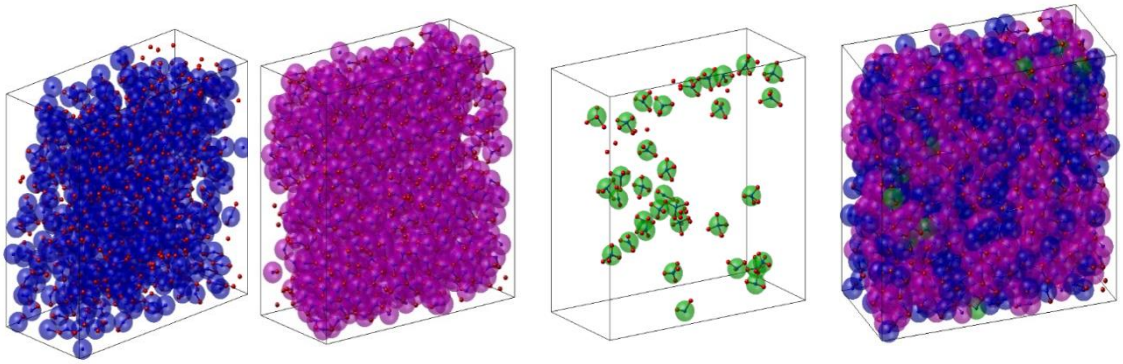

a) O-Al$_2$ *b) O-Al$_3$* *c) O-Al$_4$* *d) O-Al$_y$ (y = 2-5)*

Figure 12. The 3D visualization of the distribution of O-Al$_y$ linkage (y = 2-5) in liquid Al_2O_3 model at 0 GPa (O-Al$_2$ linkage in blue; O-Al$_3$ linkage in pink; O-Al$_4$ linkage in green and all O-Al$_y$ linkage that correspond to the snapshots from left to right.

10 GPa

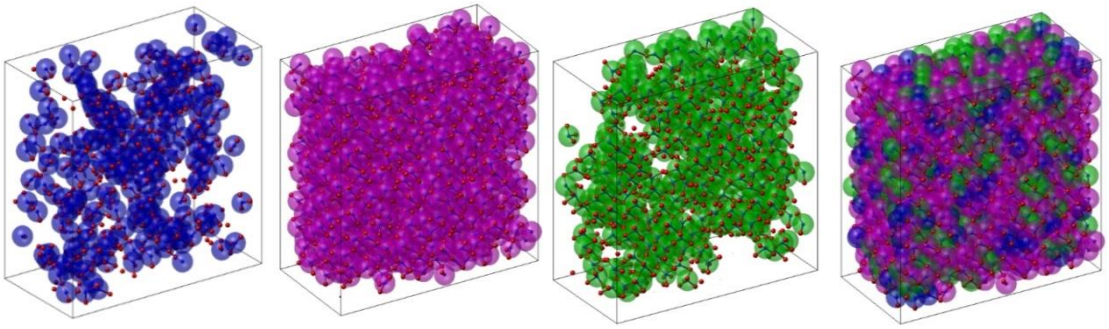

a) O-Al$_2$ *b) O-Al$_3$* *c) O-Al$_4$* *d) O-Al$_y$ (y = 2-5)*

Figure 13. The 3D visualization of the distribution of O-Al$_y$ linkage (y = 2-5) in liquid Al_2O_3 model at 10 GPa (O-Al$_2$ linkage in blue; O-Al$_3$ linkage in pink; O-Al$_4$ linkage in green and all O-Al$_y$ linkages that correspond to the snapshots from left to right.

30 GPa

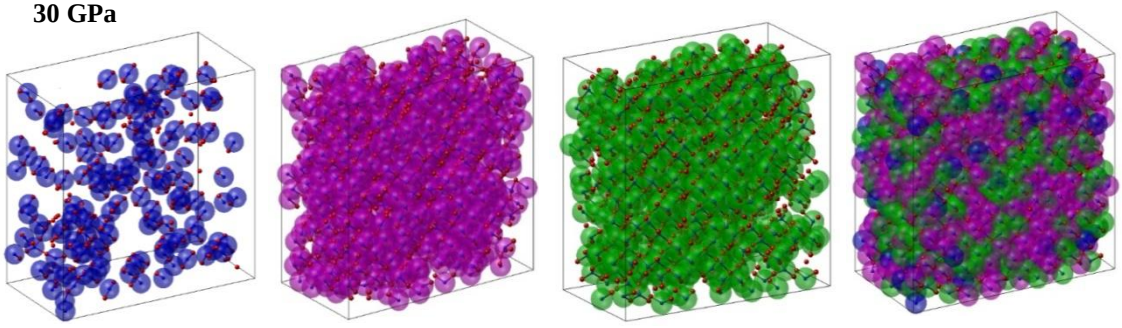

a) O-Al$_2$ *b) O-Al$_3$* *c) O-Al$_4$* *d) O-Al$_y$ (y = 2-5)*

Figure 14. The 3D visualization of the distribution of O-Al$_y$ linkage (y = 2-5) in liquid Al_2O_3 model at 30 GPa (O-Al$_2$ linkage in blue; O-Al$_3$ linkage in pink; O-Al$_4$ linkage in green and all O-Al$_y$ linkages that correspond to the snapshots from left to right.

60 GPa

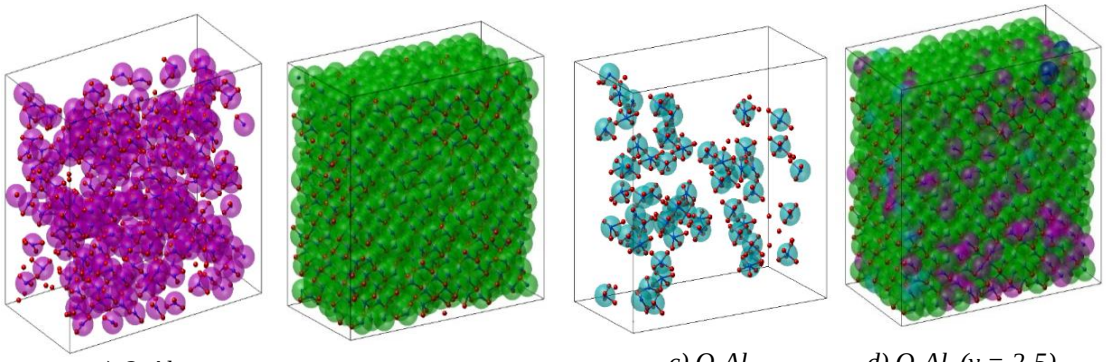

a) O-Al$_3$ *b) O-Al$_4$* *c) O-Al$_5$* *d) O-Al$_y$ (y = 2-5)*

Figure 15. The 3D visualization of the distribution of O-Al$_y$ linkage (y = 2-5) in liquid Al_2O_3 model at 60 GPa (O-Al$_3$ linkage in pink; O-Al$_4$ linkage in green; O-Al$_5$ linkage in cyan and all O-Al$_y$ linkages that correspond to the snapshots from left to right.

100 GPa

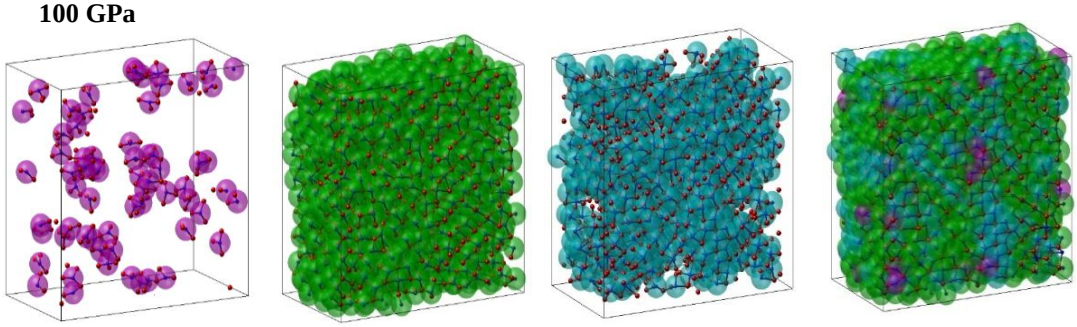

a) O-Al$_3$ *b) O-Al$_4$* *c) O-Al$_5$* *d) O-Al$_y$ (y = 3-5)*

Figure 16. The 3D visualization of the distribution of O-Al$_y$ linkage (y=2-5) in liquid Al_2O_3 model at 100 GPa (O-Al$_3$ linkage in pink; O-Al$_4$ linkage in green; O-Al$_5$ linkage in cyan and all O-Al$_y$ linkages that correspond to the snapshots from left to right.

Figure 12 displays each O atom can link to mainly two or three AlO_x polyhedrals at 0 GPa. The concentration of the tri-cluster of three AlO_x polyhedra is the largest, which is visualized by the pink regions in the model. The concentration of O-Al$_4$ in the green regions is rather small. With further increasing pressure (Figures 13 - 16), the blue regions of O-Al$_2$ linkages and pink regions of O-Al$_3$ linkages gradually replace the green regions of O-Al$_4$ linkages and the cyan regions of O-Al$_5$ linkages, respectively and the concentration of O-Al$_4$ linkages is always the largest. Moreover, we can see that the partial distribution of these regions is not uniform, thus the intermediate-range order structure is heterogeneous.

Furthermore, two adjacent AlO_x polyhedra are connected to each other through bridged oxygens to form the kind of bonds including the corner-, edge-, and face-sharing bonds that are presented in Figure 17. Figure 17 shows the dependence of the number of kinds of bonds on pressure. It can be seen that most connections are one-oxygen (corner-sharing bonds), but as the pressure increases, the number of two-oxygen connectivity increases sharply (edge-sharing bonds) while the number of three-oxygen connectivity rises slightly (face-sharing bonds).

At ambient pressure, the number of one-oxygen connectivity is considerable. There is no existence of face-sharing bonds while edge-sharing bonds account for small. At higher pressure, both the number of one- and two-connectivity are dominant while the face-sharing bonds account for a small number. Hence, under compression, the number of types of bonds increases with pressure and forming regions with different intermediate-range structures. Obviously, the change in the regions such as the yellow regions of edge-sharing bonds and the pink regions of face-sharing bonds has been clearly observed through visual images that are displayed in Figure 18. This once again shows the heterogeneity in the liquid Al_2O_3 model.

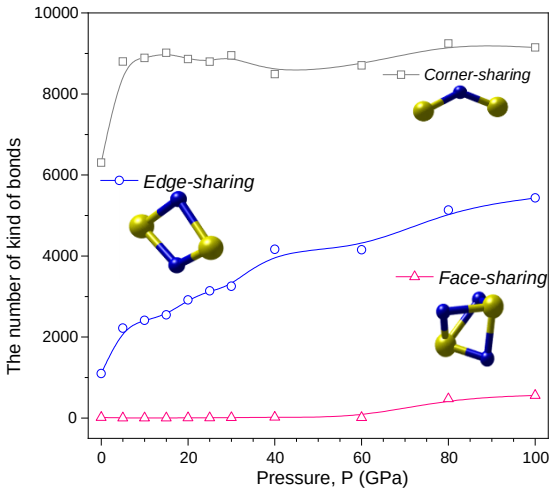

Figure 17. The distribution of the number of kind of bonds.

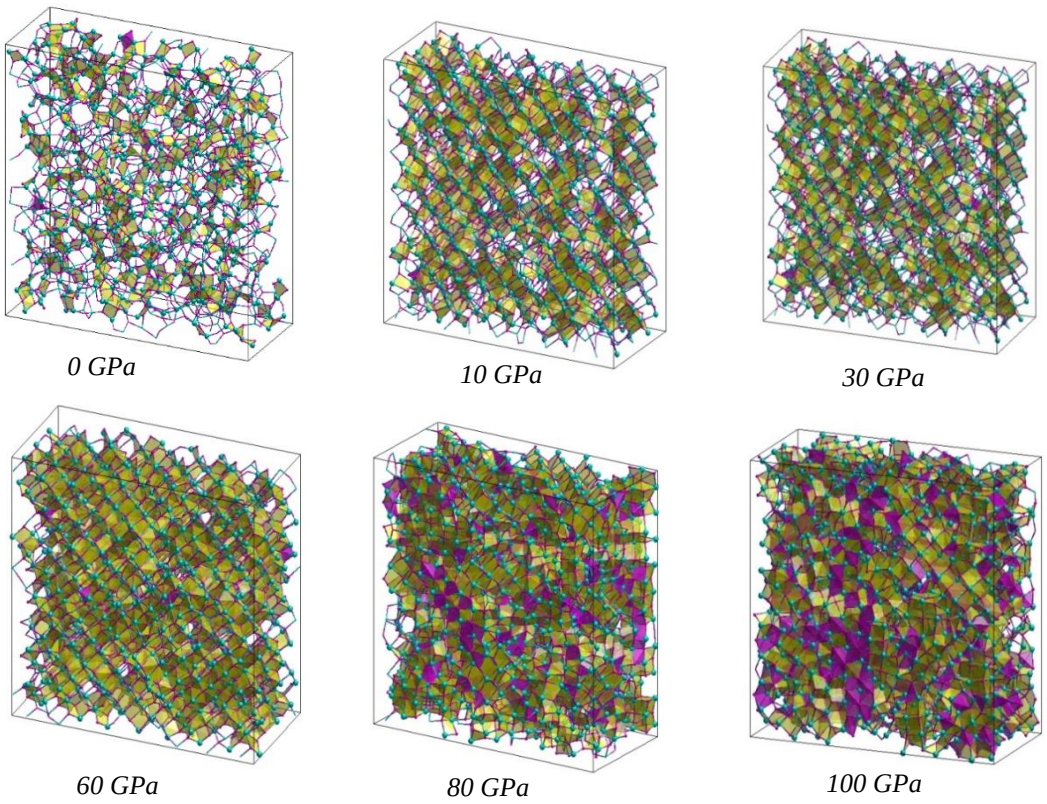

*Figure 18***.** The 3D visualization of the distribution of corner-, edge- and face-sharing bonds in liquid Al_2O_3 model. The snapshots from left to right and from top to down corresponds to 0, 10, 30, 60, 80 and 100 GPa. The edge- and face-sharing bonds are highlighted with yellow and pink color, respectively.

4. CONCLUSION

Overall, this work gives useful knowledge about the structure of liquid Al_2O_3 over broad ranges of pressure (0 - 100 GPa) through insightful intuitive data and image analysis methods. The liquid Al_2O_3 is a mixture of the region AlO_x polyhedra (x = 4 - 8) with the percentage varied with pressure. At ambient pressure, the regions with AlO_4 tetrahedra in yellow are dominant. The regions with AlO_5 pentahedra in cyan account for small. The regions with AlO_6 octahedra in pink are negligible. At 100 GPa, the structure of Al_2O_3 liquid consists of three main regions with AlO_6 octahedra in pink, AlO_7 polyhedra in red, and AlO_8 polyhedra in blue, in which the pink and red regions make up the majority.

The different regions of intermediate-range order structure are highlighted with different colors through the 3D visualization technique. The O-Al_2 and O-Al_3 linkages correspond to the AlO_4 and AlO_5 polyhedra networks. The O-Al_4 and O-Al_5 linkages correspond to the AlO_6 and AlO_7 polyhedra networks. At ambient pressure, the concentration of the tri-cluster of three AlO_x polyhedra is the largest, which is visualized by the pink regions in the model. The concentration of O-Al_4 linkages in the green regions is rather small. The number of one-oxygen connectivity is considerable. With increasing pressure, the blue regions of O-Al_2 linkages and pink regions of O-Al_3 linkages gradually replace the green regions of O-Al_4 linkages and the cyan regions of O-Al_5 linkages, respectively and the concentration of O-Al_4 linkages is always the largest. The number of one- and two-connectivity are dominant while the face-sharing bonds account for a small number. The change of the yellow regions of edge-sharing bonds and the pink regions of face-sharing bonds has been observed through visual images.

The coexistence of the different structural regions is unevenly distributed in the model, hence the structure of liquid Al_2O_3 is heterogeneous. The increased coordination is the structural densification mechanism of the liquid Al_2O_3 system under compression.

CRediT authorship contribution statement. Nguyen Van Hong, Nguyen Thi Thanh Ha and Mai Thi Lan conducted the models; Mai Thi Lan and Nguyen Thu Nhan analyzed data. Mai Thi Lan wrote the manuscript. All authors discussed the results and contributed to the final manuscript.

Declaration of competing interest. The authors declare that they have no known competing financial interests or personal relationships that could have appeared to influence the work reported in this paper.

REFERENCES

1. Roel P. - On the structure of γ-Al_2O_3, J. Catal. **392** (2020) 336-346. https://doi.org/10.1016/j.jcat.2020.10.010
2. Libor K., Mark B., János S. - High-temperature transition aluminas in δ-Al_2O_3/θ-Al_2O_3 stability range: Review, J. Catal. **393** (2021) 357-368. https://doi.org/10.1016/j.jcat.2020.10.009
3. Lawrie B. S., Adrian C. B., Philip S. S., Louis H., Henry E. F., Chris J. B., Shinji K., Richard W. J. K., Aleksei B., Martin C. W., *et al.* - Joint diffraction and modeling approach to the structure of liquid alumina, Phys. Rev. B **87** (2013) 024201. https://doi.org/10.1103/PhysRevB.87.024201
4. Caracas.R and Cohen R.E. - Prediction of a new phase transition in Al_2O_3 at high pressures, Geophysical Research Letter **32** (2005) L06303. https://doi.org/10.1029/2004GL022204.

5. Artem R. O. and Shigeaki O. - The high-pressure phase of alumina and implications for Earth's D'' layer, PNAS **102** (2005) 10828-10831. https://doi.org/10.1073/pnas.0501800102
6. Perevalov T. V., Gritsenko V. A., and Kaichev V. V. - Electronic structure of aluminum oxide: ab initio simulations of α and γ phases and comparison with experiment for amorphous films, Eur. Phys. J. Appl. Phys. **52** (2010) 30501.https://doi.org/10.1051/epjap/2010159
7. Ansell S. - Structure of Liquid Aluminum Oxide, Phys. Rev. Lett. **78** (3) (1997) 464-466. https://doi.org/10.1103/PhysRevLett.78.464
8. Lampartera P., Kniep R. - Structure of amorphous Al_2O_3, Physica B Condens, Matter. **234-236** (1997) 405-406. https://doi.org/10.1016/S0921-4526(96)01044-7
9. Landron C., Hennet L., Jenkins T. E., Greaves G. N., Coutures J. P., and Soper A. K. - Liquid Alumina: Detailed Atomic Coordination Determined from Neutron Diffraction Data Using Empirical Potential Structure Refinement, Phys. Rev. Lett. **86** (21) (2001) 4839-4842. https://doi.org/10.1103/PhysRevLett.86.4839
10. Caijuan S., Oliver L. G. A., Diana B., Jincheng D., Joerg N., Anthony T., Richard W. J. K., Jinglin Y. and Chris J. B. - The Structure of Amorphous and Deeply Supercooled Liquid Alumina, fmats. **6** (2019) 1-15. https://doi.org/10.3389/fmats.2019.00038.
11. Sung K. L., Sung B. L., Sun Y. P., Yoo S. Y., and Chi W. A. - Structure of Amorphous Aluminum Oxide, PRL. **103** (2009) 095501.https://doi.org/10.1103/PhysRevLett.103.095501.
12. Deng H., Fangming L., Shixue G., Duanwei H. - High-pressure work hardening of alumina, Ceram. Int. **47** (2021) 19989-19994. https://doi.org/ 10.1016/j.ceramint.2021.04.009.
13. Zhongwu W., Huahai M., Saxenaa S.K. - The melting of corundum (Al_2O_3) under high pressure conditions, J. Alloys Compd. **299** (2000) 287-291. https://doi.org/10.1016/S0925-8388(99)00794-X
14. Rajeev A., Belonoshko A. B. and Bo¨rje J. - Melting and liquid structure of aluminum oxide using a molecular-dynamics simulation, Phys Rev E **57**(2) (1998) 1673-1676. https://doi.org/10.1103/PhysRevE.57.1673
15. Vashishta P., Kalia R. K., Nakano A., *et al*. - Interaction potentials for alumina and molecular dynamics simulations of amorphous and liquid alumina, J. Appl. Phys. **103** (2008) 083504. https://doi.org/10.1063/1.2901171
16. Gonzalo G., Belonoshko A. B., Rajeev A., and Bo¨rje J. - Structural properties of liquid Al2O3: a molecular dynamics study, Phys. Rev. E **61** (3) (2000) 2723-2729. https://doi.org/10.1103/PhysRevE.61.2723
17. Hoang V. V. - About an order of liquid–liquid phase transition in simulated liquid Al_2O_3, Phys Lett. A **335** (2005) 439-443. https://doi.org/10.1016/j.physleta.2004.12.040
18. Hemmati M. - Structure of liquid Al_2O_3 from a computer simulation model, J. Phys. Chem. B **103** (1999) 4023-4028. https://pubs.acs.org/doi/abs/10.1021/jp983529f
19. Jahn S., Madden P. A. - Structure and dynamics in liquid alumina: simulations with an ab initio interaction potential, J. Non-Cryst Solids **353** (32 - 40) (2007) 3500-3504. https://doi.org/10.1016/j.jnoncrysol.2007.05.104

20. Kien P. H., An P. M., and Trang G. T. T. - The structural transition under compression and correlation between structural and dynamical heterogeneity for liquid Al_2O_3, Int. J. Mod. Phys. B **33** (31) (2019) 1950380. https://doi.org/10.1142/S0217979219503806
21. Kien P. H., Nhu T. T. Q., Trang G. T. T. - Characterization of Structural Transition and Heterogeneity under Compression for Liquid Al_2O_3 Using Molecular Dynamics Simulation, HIJ. **3** (2) (2022). https://hightechjournal.org/index.php/HIJ/article/view/215